The Astrophysical Journal, 826:182 (10pp), 2016 August 1 doi:10.3847/0004-637X/826/2/182
© 2016. The American Astronomical Society. All rights reserved.

A NUMERICAL SIMULATION OF COSMIC RAY MODULATION NEAR THE HELIOPAUSE. II. SOME PHYSICAL INSIGHTS

Xi Luo[1,2], Marius S. Potgieter[2], Ming Zhang[3], Nikolai V. Pogorelov[4], Xueshang Feng[1], and R. du Toit Strauss[2]
[1] SIGMA Weather Group, State Key Laboratory of Space Weather, National Space Science Center, Chinese Academy of Sciences, Beijing 100190, China
[2] Centre for Space Research, North-West University, Potchefstroom 2520, South Africa
[3] Department of Physics and Space Sciences, Florida Institute of Technology, 150 West University Boulevard, Melbourne, FL 32901, USA
[4] Department of Physics and Center for Space Plasma and Aeronomic Research, University of Alabama in Huntsville, 301 Sparkman Dr., Huntsville, AL 35899, USA
Received 2015 November 17; revised 2016 May 17; accepted 2016 May 27; published 2016 July 29

ABSTRACT

Cosmic ray (CR) transport near the heliopause (HP) is studied using a hybrid transport model, with the parameters constrained by observations from the *Voyager 1* spacecraft. We simulate the CR radial flux along different directions in the heliosphere. There is no well-defined thin layer between the solar wind region and the interstellar region along the tail and polar directions of the heliosphere. By analyzing the radial flux curve along the direction of *Voyager 2*, together with its trajectory information, the crossing time of the HP by *Voyager 2* is predicted to be in 2017.14. We simulate the CR radial flux for different energy values along the direction of *Voyager 1*. We find that there is only a modest modulation region of about 10 au wide beyond the HP, so that *Voyager 1* observing the Local Interstellar Spectra is justified in numerical modeling. We analyze the heliospheric exit information of pseudo-particles in our stochastic numerical (time-backward) method, conjecturing that they represent the behavior of CR particles, and we find that pseudo-particles that have been traced from the nose region exit in the tail region. This implies that many CR particles diffuse directly from the heliospheric tail region to the nose region near the HP. In addition, when pseudo-particles were traced from the Local Interstellar Medium (LISM), it is found that their exit location (entrance for real particles) from the simulation domain is along the prescribed Interstellar Magnetic Field direction. This indicates that parallel diffusion dominates CR particle transport in the LISM.

Key words: cosmic rays – Sun: heliosphere

1. INTRODUCTION

Cosmic rays (CRs) are one of the important probes for detecting the properties of the interplanetary and the interstellar medium since the interaction with the background medium enables them to carry information about the background medium. Recently, CR observations have been one of the main signatures of the historical event of *Voyager 1*'s crossing of the heliopause (HP) and entering the Local Interstellar Medium (LISM) in 2012 August (Gurnett et al. 2013; Stone et al. 2013). The spacecraft simultaneously detected a rapid increase (jump) in the galactic CR flux and a large decrease in the anomalous CR flux (Krimigis et al. 2013; Webber & McDonald 2013). Since then, the CR intensities at all energy levels have been observed to be nearly constant.[5]

These observations near the HP have also motivated several CR numerical simulations. For example, by using a pitch-angle diffusion transport equation, Strauss & Fichtner (2014) and Florinski et al. (2013) studied the CR anisotropy observed by *Voyager 1* when crossing the HP; Florinski et al. (2015) investigated the dependence of the CR anisotropy on rigidity near the HP and attributed it to gradient drifts; assuming that the first adiabatic invariant is conserved, Jokipii & Kóta (2014) interpreted the galactic CR disturbance observed in the LISM in 2013 March as caused by the Interstellar Magnetic Field (IMF) disturbance reported by Burlaga et al. (2013). Luo et al. (2015) reproduced the CR flux jump observed by *Voyager 1* in 2012 August with their hybrid CR transport model by modifying the ratio of $\kappa_{\parallel}/\kappa_{\perp}$, where $\kappa_{\parallel}$ ($\kappa_{\perp}$) denotes the parallel (perpendicular) diffusion coefficient.

[5] From http://voyager.gsfc.nasa.gov/.

Presently, some open questions concerning CR behavior near and beyond the HP remain. For example, is the HP truly the modulation boundary or is some modulation happening beyond the HP? Scherer et al. (2011) and Strauss et al. (2013) first demonstrated that CRs could already be modulated in principle beyond the HP, depending on their energy and the ratio of $\kappa_{\parallel}/\kappa_{\perp}$, while Kóta & Jokipii (2014) argued that such modulation should be completely negligible beyond the HP, assuming that the diffusion coefficient in the outer heliosheath is very large. We will address this question in more detail by using model parameters that are constrained by *Voyager 1* observations. Another crucial question is how the radial flux varies along other directions instead of *Voyager 1*'s, in particular whether *Voyager 2* would observe a similar jump in the radial flux near the HP. Webber & Intriligator (2015) used low-energy CR data from *Voyager 1* and *2* to predict that *Voyager 2* could encounter the HP very soon. In this study, we follow our previous numerical approach to also make a prediction in this context. In addition, we trace the trajectories of individual pseudo-particles in phase space in order to investigate and establish how individual CR particles could be transported near the HP in order to gain insight and a better understanding of the modulation process.

The paper is structured as follows. The numerical method is briefly presented in Section 2, followed by simulation results in Section 3 with discussions on the questions mentioned above. Conclusions are presented in Section 4.

2. NUMERICAL APPROACH

Given that the observed CR anisotropy beyond the HP is less than 10%, we still believe that Parker's transport equation (Parker 1965) can fulfill our intent to understand the large-scale

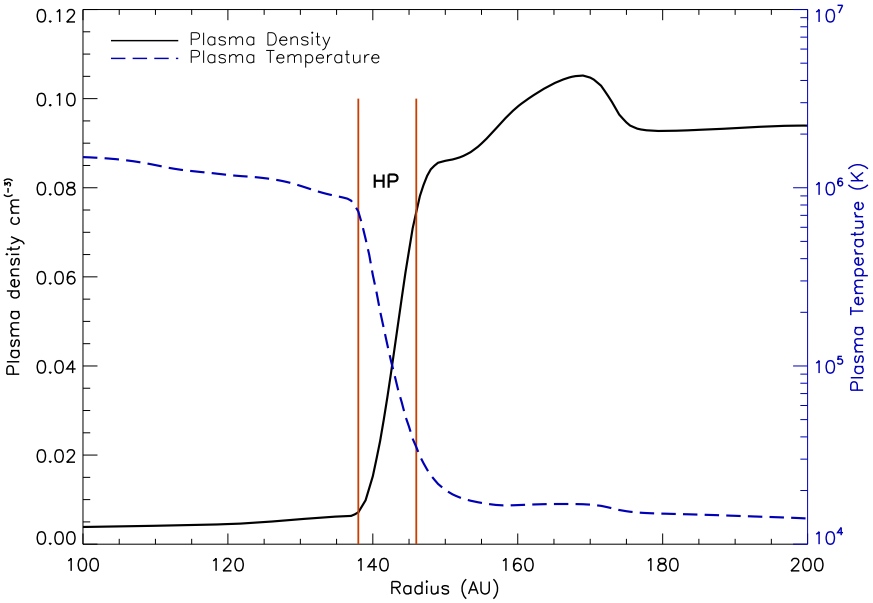


Figure 1. Plasma density (cm^{-3}) and temperature (K) along the *Voyager 1* direction in the MHD data. The HP is a region with a width of about 10 au.

CR transport behavior near the HP. We therefore continue to base our numerical study on this equation:

$$\frac{\partial f}{\partial t} = -(\boldsymbol{V} + \langle \boldsymbol{V}_D \rangle) \cdot \nabla f + \nabla \cdot (K^{(s)} \cdot \nabla f) + \frac{1}{3}(\nabla \cdot \boldsymbol{V}) \frac{\partial f}{\partial \ln p}. \quad (1)$$

Here, $f(\boldsymbol{r}, p, t)$ is the distribution function or the phase-space density as a function of spatial position $\boldsymbol{r}$, momentum p, and time t. The flux $j_T \propto p^2 f$.

Parker's equation contains the solar wind convection speed $\boldsymbol{V}$, the average particle drift speed $\langle \boldsymbol{V}_D \rangle$ in the non-uniform Heliospheric Magnetic Field (HMF), and the diffusion tensor $K^{(s)} = \kappa_\perp I + (\kappa_\parallel - \kappa_\perp)\hat{b}\hat{b}$. Note that $\kappa_\perp(\kappa_\parallel)$ is the diffusion coefficient perpendicular (parallel) to the ambient magnetic field, I is the unit tensor, and $\hat{b}$ is the unit vector along the magnetic field direction. The last term $\frac{1}{3}(\nabla \cdot \boldsymbol{V})\frac{\partial f}{\partial \ln p}$ in Equation (1) is the momentum change term, which describes the adiabatic cooling process.

Following Zhang (1999), Equation (1) is described in its Stochastic Differential Equation form:

$$d\boldsymbol{X} = (\nabla \cdot K^{(s)} - \boldsymbol{V} - \langle \boldsymbol{V}_D \rangle) ds + \sum_\sigma \boldsymbol{\alpha}_\sigma dW_\sigma(s), \quad (2)$$

$$dp = \frac{1}{3} p (\nabla \cdot V) ds. \quad (3)$$

In the above equation, $dW_\sigma(s)$ is the Wiener process, and it obeys the following Gaussian Distribution:

$$P(dW_\sigma(s)) = \frac{1}{\sqrt{2\pi ds}} \exp\left[-\frac{dW_\sigma^2(s)}{2ds}\right]. \quad (4)$$

This set of Stochastic Differential Equations can be integrated to describe the trajectories of individual pseudo-particles in the phase space. In order to get a steady-state solution of $f(\boldsymbol{r}, p)$, a large number of pseudo-particles are traced from a given $(\boldsymbol{r}, p)$ until they reach the simulation boundary $\boldsymbol{r}_b$ with a value of $f_b(\boldsymbol{r}_b, p_b)$ for the first time. By performing an ensemble average, we obtain $f(\boldsymbol{r}, p) = \langle f_b(\boldsymbol{r}_b, p_b) \rangle$. For details of this numerical method see also e.g., Kopp et al. (2012).

Following Luo et al. (2015), we choose the following forms for the diffusion coefficients $\kappa_\parallel$ and $\kappa_\perp$:

$$\kappa_\parallel = \kappa_{\parallel 0} \beta \left(\frac{p}{p_0}\right)^{0.5} \frac{B_{\rm eq}}{B} \times fac, \quad (5)$$

$$\kappa_\perp = \kappa_{\perp 0} \beta \left(\frac{p}{p_0}\right)^{0.5} \frac{B_{\rm eq}}{B} / fac; \quad (6)$$

and

$$fac = \frac{1 + M_k}{2} + \frac{M_k - 1}{2} \times \frac{(B/B_{\rm ism})^6 - (B_{\rm ism}/B)^6}{(B/B_{\rm ism})^6 + (B_{\rm ism}/B)^6}. \quad (7)$$

In these equations, B is the local magnetic field magnitude, $B_{\rm ism}$ is the magnetic field magnitude in the interstellar medium, and $B_{\rm eq}$ is the magnetic field magnitude near the Earth. M_k, $\kappa_{\perp 0}$, and $\kappa_{\parallel 0}$ are treated as constants and β is the ratio of particle speed to the speed of light. The p_0 parameter is a reference momentum (in our case 1 GeV/c).

The purpose of Equation (7) is to avoid the sharp transition for $\kappa_\parallel$ and $\kappa_\perp$ as they are increased in the outer heliosheath. As demonstrated by Figure 2, diffusion coefficients vary in a relatively wider region. Thus, without a singularity problem, we can still calculate the $\nabla \cdot K^{(s)}$ term in Equation (2) when the ratio of $\kappa_\parallel/\kappa_\perp$ is significantly magnified beyond the HP.

Our numerical method involves a hybrid CR transport code as described in detail by Luo et al. (2013). The global heliospheric features, containing the HMF and solar wind speed, are obtained from executing a MHD plasma/multi-fluid neutral atom model (Pogorelov et al. 2013). As such, a snapshot of MHD data corresponding to the epoch when *Voyager 1* crossed the HP was taken from a series of time-varying output data, which was then incorporated into the transport equation to arrive at solutions applicable to CR modulation as discussed by Luo et al. (2013). A similar approach was followed by Strauss et al. (2013).

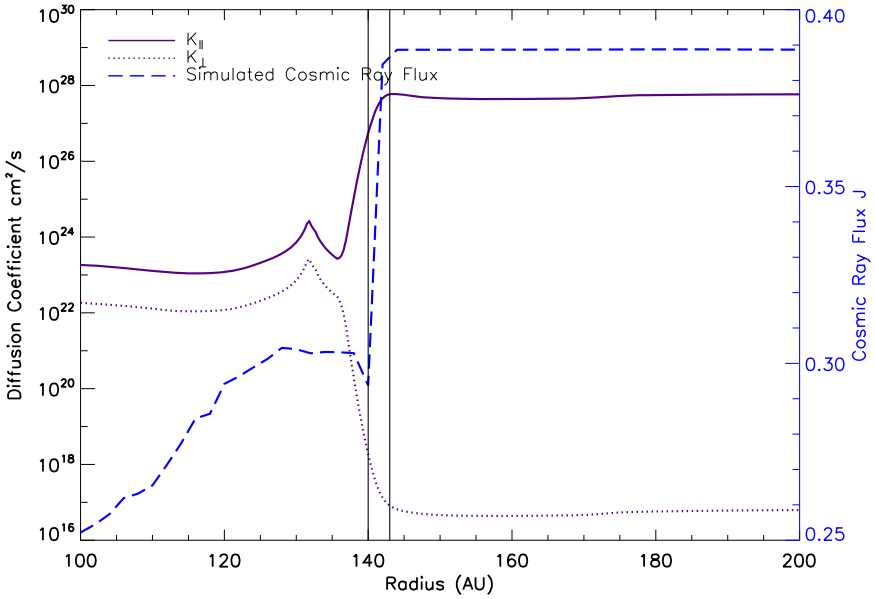


Figure 2. Magnified diffusion coefficients and the simulated cosmic ray flux along the assumed *Voyager 1* direction. The cosmic ray flux jump is a region with a width of about 3 au (141–144 au).

Within the limitation of our numerical MHD modeling, the HP is smeared out and quite broad in this MHD model. Figure 1 shows the plasma density and temperature variation (from the MHD data) along the assumed *Voyager 1* direction (polar angle $\theta = 56°$, azimuthal angle $\phi = 4°$). By setting a threshold, the HP along the assumed *Voyager 1* direction is defined as the region from 138 to 146 au (Luo et al. 2015). However, it was found that after the diffusion coefficients beyond the HP are significantly magnified, the simulated CR flux jumps over a much thinner region as illustrated in Figure 2. Thus, in this study we define the HP as the region where the CR flux jumps upward. Along the assumed *Voyager 1* direction, this region is from 141 to 144 au.

The simulation outer boundary is a sphere, outside which the CRs are not influenced by solar activity. Theoretically, the whole MHD heliosphere model should be inside this boundary, but the resulting computing is too time consuming. Thus, in our numerical simulation, the radius of this sphere is set at 300 au to achieve the optimal balance between the computation speed and numerical accuracy.

3. RESULTS AND DISCUSSION

The *Voyager 1* crossing of the HP in 2012 August provided us for the first time with in situ observational data that can be used to constrain the numerical modeling of CRs, the main theme of this work, in the vicinity of the HP. Luo et al. (2015) could reproduce the basic trends of these observations and found that the ratio $\kappa_{\parallel}/\kappa_{\perp}$ needs to be magnified by a factor of 10^{10} across the HP so that $\kappa_{\parallel}$ reaches the magnitude of $10^{27}\,\mathrm{cm^2\,s^{-1}}$ beyond the HP, which nearly reaches the value used in GALPROP, a well-known galactic propagation model (Strong et al. 2007). Recent magnetic field observations from *Voyager 1* (Burlaga et al. 2014) and inferred from the reported *IBEX* ribbon (Gamayunov et al. 2010) suggest a very low turbulence level for the very local ISM, consistent with large $\kappa_{\parallel}$ and low $\kappa_{\perp}$ values beyond the HP. Thus, we are convinced that our parameter setup can realistically reflect the modulation situation near the HP. The default parameter setup is $\kappa_{\parallel 0} = 50 \times 10^{20}\,\mathrm{cm^2\,s^{-1}}$, $\kappa_{\perp_0} = 5 \times 10^{20}\,\mathrm{cm^2\,s^{-1}}$ in Equations (6) and (7); $M_k = 1$, if $r \leqslant r_{\mathrm{hp}} - 10$ and $M_k = 10^5$ if $r > r_{\mathrm{hp}} - 10$ (r_{hp} is the upper limit of the MHD HP region). So the ratio $\kappa_{\parallel}/\kappa_{\perp} = 10$ inside the HP and it gradually approaches 10^{10} beyond the HP as shown in Figure 2. In the following, we use this setup to study the behavior of CRs near the HP as mentioned above with the specific intention to relate our simulations to *Voyager 1* CR observations.

3.1. CR Radial Flux along a Different Direction

In Figure 3 the simulated radial flux of 200 MeV protons is shown in seven different heliospheric directions. As before, we find a clearly defined large upwards jump in the radial flux at the HP along *Voyager 1*'s direction (polar angle $\theta = 56°$, azimuthal angle $\phi = 4°$). Similar jumps, which imply very large radial gradients across the HP, are also found along the simulated *Voyager 2* direction (polar angle $\theta = 120°$, azimuthal angle $\phi = 40°$), in the nose direction (polar angle $\theta = 90°$, azimuthal angle $\phi = 0°$), and in the direction of the heliospheric flanks (polar angle $\theta = 90°$, azimuthal angle $\phi = 90°$). Since *Voyager 2* must still cross the HP, perhaps in the near future (Richardson & Decker 2014) it would be worthwhile to pay more attention to the simulated radial flux in *Voyager 2*'s direction.

First, some conjecturing: *Voyager 2* crossed the Termination Shock (TS) in the year 2007.66 at a distance of 83.7 au from the Sun (Stone et al. 2008). It is moving away from the Sun with a speed of 3.3 au year^{-1}. For the region beyond the TS, we can approximate the relationship between the actual time of the year (time) and *Voyager 2*'s distance (radius) as

$$\mathrm{time} = (\mathrm{radius} - 83.7\ \mathrm{au})/3.3\ \mathrm{year} + 2007.66\ \mathrm{year}. \quad (8)$$

However, because there is a well-known overestimation of the width of the inner heliosheath in our MHD model, we need to consider the following: *Voyager 1* crossed the HP at a distance of 122 au in 2012.65; the HP in our MHD model along *Voyager 1* is around 141 au, causing a 19 au overestimation.

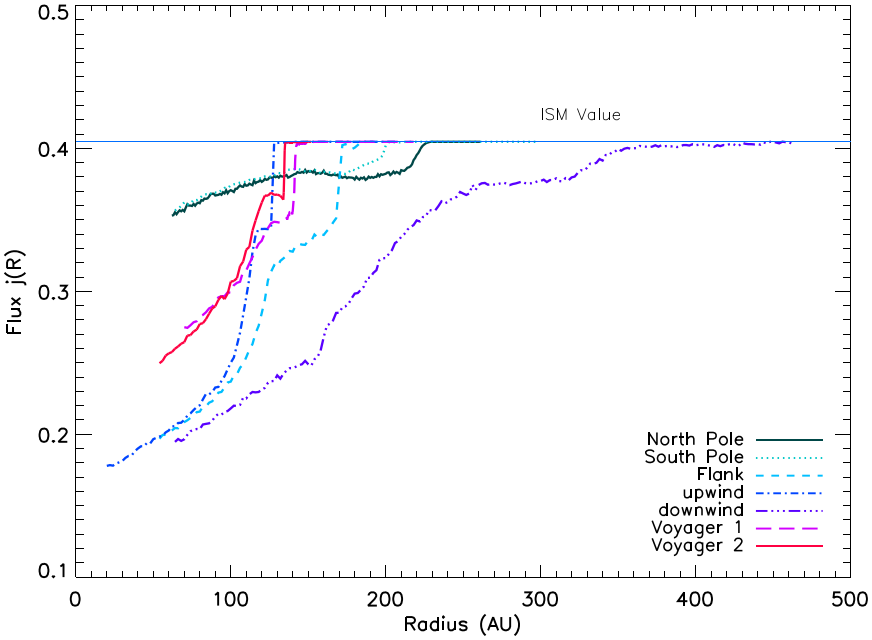


Figure 3. Simulated 200 MeV galactic CR proton flux $j(R)$ as a function of radial distance along different directions: poles, flank, upwind, downwind, and for *Voyager 1* and *Voyager 2*. Here, the flank direction denotes the direction that is on the *X*–*Y* ecliptic plane and has 90° with respect to the upwind direction. The unit for the flux is arbitrary, which is also applied to Figures 4–6.

Assuming that the overestimation along the directions of both *Voyager 1* and *Voyager 2* is the same, we can modify Equation (8) as

$$\text{time} = [(\text{radius}_{\text{MHD}} - 19\ \text{au}) - 83.7\ \text{au}]/3.3\ \text{year} + 2007.66\ \text{year}. \quad (9)$$

Based on our simulation results, the CR flux along *Voyager 2* should make the predicted jump at about 134 au, which is a scaled value of 115 au. Plugging this value into Equation (9), the estimated time for this jump is predicted to occur around the year of 2017.14.

As shown in Figure 3, the jump in the simulated CR flux along the polar and the downwind direction is much weaker and the region over which the jump occurs in the model is spread out so that the modulation boundary is less clearly defined. Zhang et al. (2015) pointed out that the galactic CR flux value near the HP is attributed to the balance between the flux from the heliosphere and the interstellar medium. Thus, as shown here, the HP is not a well-defined relatively thin layer in the tail or polar direction but could extend over a larger region (tens of au) where the CR flux is controlled by the flow both from the heliosphere and the LISM.

3.2. The CR Modulation Boundary

Galactic CRs, when entering the heliosphere, are modulated by conditions caused by solar activity. To properly simulate this process a heliospheric boundary must be specified. Whether or not the HP can be assumed to be this outer spatial boundary is under debate (Scherer et al. 2011; Strauss et al. 2013, 2015; Kóta & Jokipii 2014; Strauss & Potgieter 2014). Luo et al. (2015) illustrated and confirmed that, in principle, modulation beyond the HP is possible but strongly depends on what is assumed for the diffusion coefficients across the HP (as demonstrated by Figure 4). In what follows, we take this investigation further, but from a different point of view, by constraining the modulation parameter setup using *Voyager 1* CR observations inside and outside the HP. The modeling studies done so far were based on simply assuming these parameters within the limited knowledge we have about them.

As demonstrated above, the CR radial flux experiences a significant increase (jump) near the HP depending on where it is crossed, a feature that we now consider to be characteristic of the model. Recently, Webber & Quenby (2015b) even stated that the CR flux jump observed by *Voyager 1* near the HP may account for $\sim 1/3$ of the total solar modulation, depending on the energy considered. In Figure 5 this jump is demonstrated again for 200 MeV protons. This intensity jump is only present in CR modulation models that include an outer heliosheath, and cannot be reproduced by the traditional models that prescribe the Local Interstellar Spectra (LIS) exactly at the HP. Beyond this jump, a relatively narrow region (about 10 au) exists beyond the HP where very modest modulation occurs. It can be argued that since disturbances created by solar activity can propagate beyond the HP as is now observed (Gurnett et al. 2015; Intriligator et al. 2015), this region could also change to some degree. The lower panel of Figure 5 manifests this aspect by showing how the computed CR radial gradient varies over this region with a value of about 0.015% per au before it becomes essentially zero (the blue crosses illustrate the actual simulation results and the black line is the linear fit to these simulation points). This value of 0.015% per au is an order of magnitude less than the typical values for the inner heliosphere (Luo et al. 2013).

We also simulated the radial flux for the lower energy CR particles (50, 10, and 5 MeV) as displayed in Figure 6. As in the previous figure layout, the three lower panels manifest the flux variation near the HP. The values of the radial gradients for these lower energy CRs can approach 0.02% per au, but the width for this modest modulation region remains about 10 au.

We emphasize that to reproduce these small radial gradients the diffusion coefficients must have the values

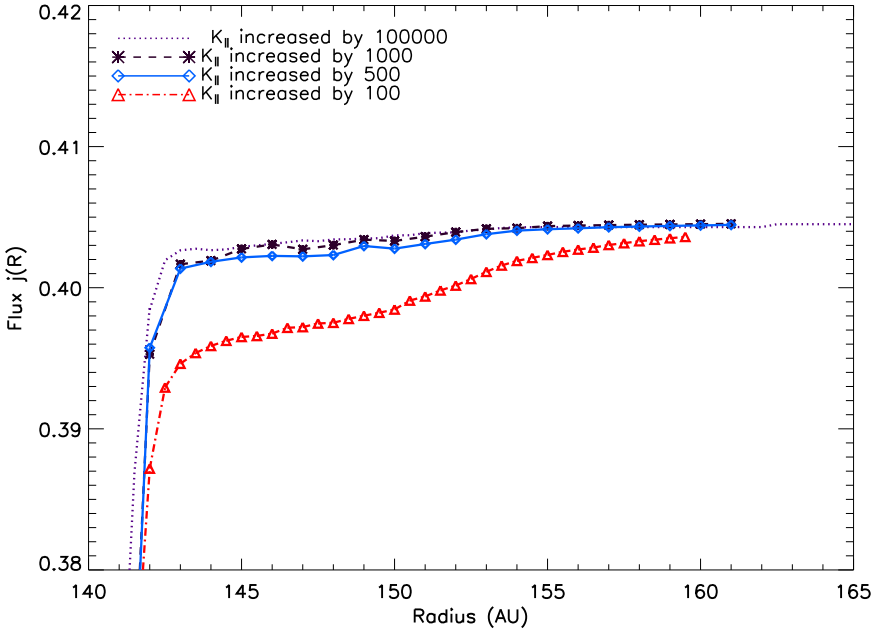


Figure 4. Simulated 200 MeV proton radial flux along the *Voyager 1* direction for different modifications of $\kappa_{\parallel}$ in the LISM. In these four cases, $\kappa_{\perp}$ is set to decrease by 10^5 in the LISM, while $\kappa_{\parallel}$ is increased by 10^5, 10^3, 5×10^2, and 10^2, respectively.

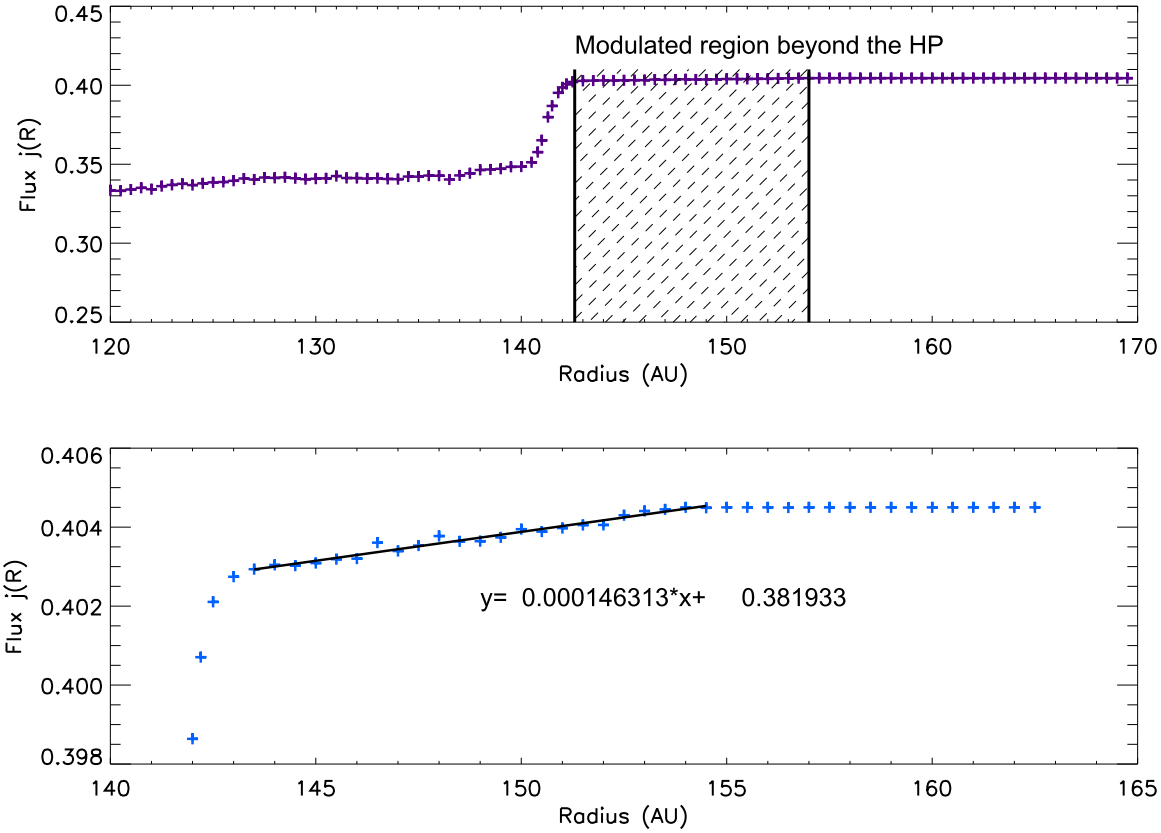


Figure 5. Simulated 200 MeV CR proton flux along the *Voyager 1* direction. The lower panel illustrates the flux just beyond the HP: the blue crosses are the simulation values and the solid black line is obtained from a linear fit for these simulation values. The fitted linear equation is also shown in the plot.

$K_{\parallel} \simeq 10^{27}\ \mathrm{cm^2\,s^{-1}}$, $K_{\perp} \simeq 10^{17}\ \mathrm{cm^2\,s^{-1}}$, and $K_{rr} \simeq 10^{26}\ \mathrm{cm^2\,s^{-1}}$. A smaller value would produce far larger radial gradients beyond the HP and is illustrated in Figure 4. It is shown that as we reduce the magnifying factor of $K_{\parallel}$ in the LISM, the CR radial gradient beyond the HP becomes larger. For example, the radial gradient in the ISM can be as large as 0.13% per au (nearly an order of magnitude larger than previous value 0.015%) if $K_{\parallel}$ only reaches $10^{24}\ \mathrm{cm^2\,s^{-1}}$ in the LISM. Similar features were also illustrated by Strauss et al. (2013).

Although the CR flux observed by *Voyager 1* beyond the HP is nearly constant, it does not rule out the existence of this modest modulation region: there are indications of small radial

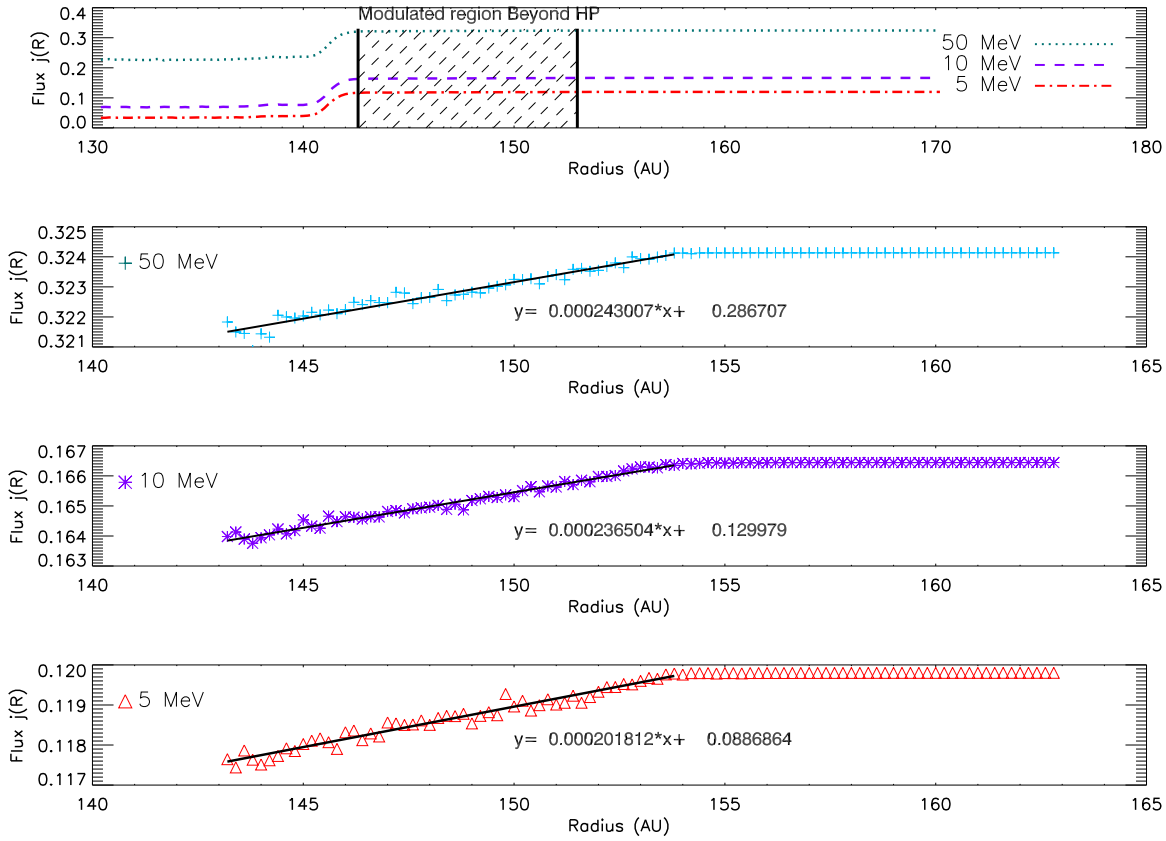


Figure 6. Simulated 50, 10, and 5 MeV CR proton radial fluxes along the *Voyager 1* direction, for a layout similar to the previous figure.

gradients in the reported *Voyager 1* CR observations (J. D. Richardson 2015, private communication). In addition, there is evidence for the remnant of a shock traveling from the inner heliosphere being observed in the interstellar medium (Burlaga et al. 2013) and its effect on CR transport (Jokipii & Kóta 2014; Gurnett et al. 2015). Thus, it is quite reasonable that CRs will still be affected by solar activity at least in a small region just beyond the HP. However, based on our simulation, the width of this region is about 10 au with the modulation level fairly small. This contributes less than 1% of the total modulation from the HP to the Earth.

3.3. Exit Momentum and Locations of Pseudo-particles

Based on the stochastic method as utilized here, we are able to trace individual pseudo-particle trajectories. Inspecting them sometimes gives surprising insights. Since the pseudo-particles have the same distribution as real particles entering at the modulation boundary, for a case of little modulation near the HP region, we can approximate the behavior of these pseudo-particles as that of real particles. In what follows, we investigate the characteristic behavior of exiting pseudo-particles, that is, we interpret them as real particles entering the heliosphere in order to reach the position of *Voyager 1*. It enables us to gain understanding of the physical processes involved.

The red dots in Figure 7 demonstrate the exit locations for 200 MeV pseudo-particles that had started at 145 au along the *Voyager 1* direction. These results are interpreted as demonstrating the heliospheric entering location for galactic protons that arrive at this particular position. The left panels show the case where we do not modify the ratio $\kappa_{\|}/\kappa_{\perp}$, whereas the panel on the right side illustrates the situation after we have increased the ratio by 10^{10} in the outer heliosheath. The displayed axes follow the coordinate system as defined in our MHD simulation: the *Z*-axis is along the Sun's rotation axis, and the *X*-axis is along the opposite unperturbed LISM velocity vector, while the *Y*-axis completes this right-hand XYZ coordinate system. Thus, the nose (tail) region is on the positive (negative) part of the *X*-axis. This is also labeled in the upper left plot.

In the simulation, in order to obtain the two upper plots, the simulation outer boundary is manually set at 300 au. As illustrated by the left panel of Figure 8, the HMF spiral lines, inside the inner heliosheath, may extend fully from the nose region to the boundary location of about 300 au in the tail region, enabling pseudo-particles to diffuse along these lines from the tail region to the nose region. The upper left plot of Figure 7 is the case when the $\kappa_{\|}/\kappa_{\perp}$ ratio is not increased in the outer heliosheath. By counting the number of red dots, the ones on the positive side of the *X*-axis (nose region) account for only 9% of the total.

That means few pesudo-particles penetrate outward directly from the nose region, and most pseudo-particles exit from the tail region. As $\kappa_{\|}/\kappa_{\perp}$ increases (upper right panel), the percentage of the red dots on the positive part decreased to 4%. Because of the more efficient parallel diffusion along the magnetic field lines, a large number of pseudo-particles exit from the tail region. This indicates that most CR particles could enter the heliosphere from the tail region, following the spiral magnetic field lines and being observed by *Voyager 1* in the nose region. Similar features have also been reported by McComas & Schwadron (2012) and Strauss et al. (2013).

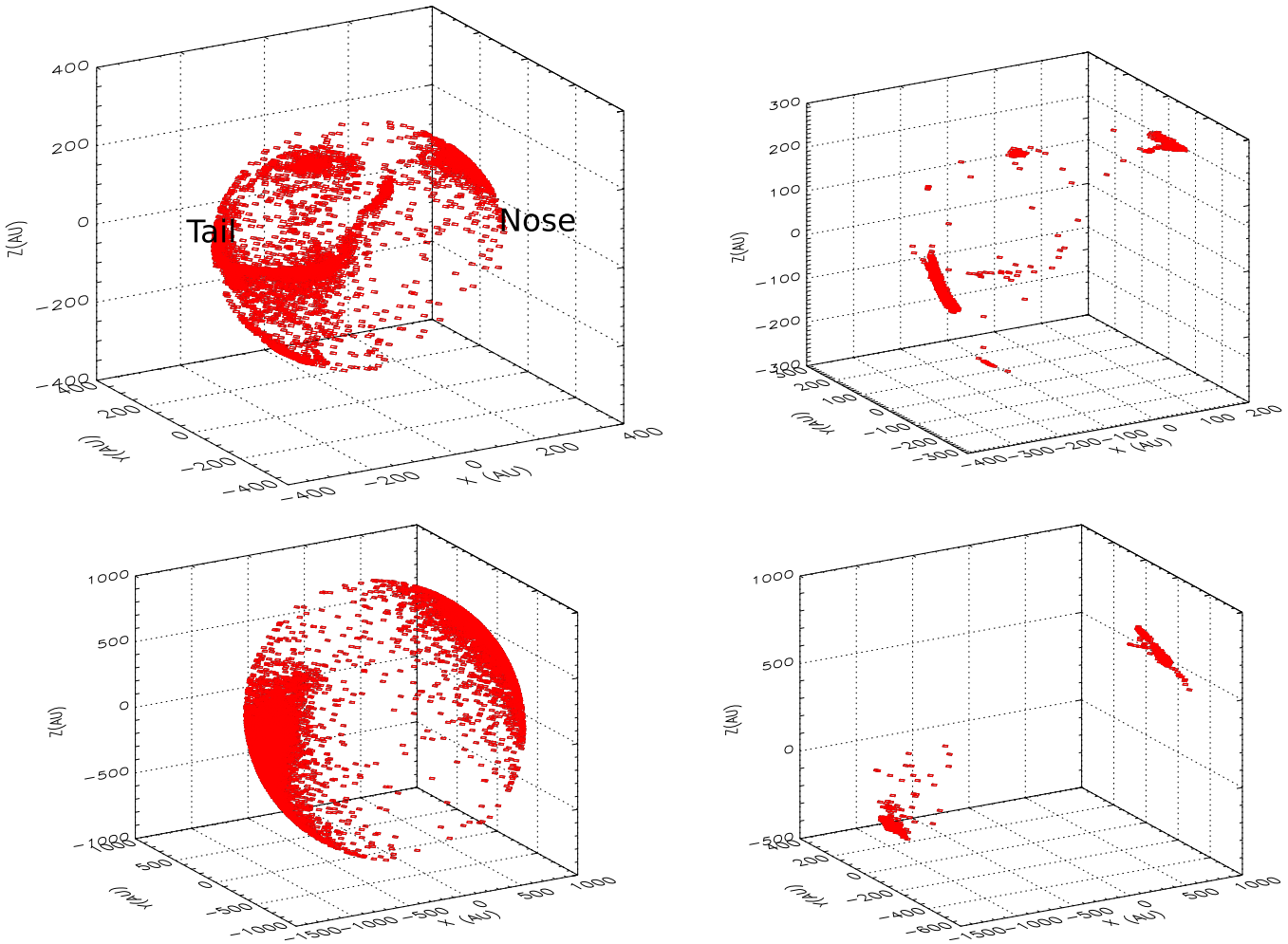


Figure 7. In this figure the red points exhibit the exit locations in au for 200 MeV pseudo-particles that started at 145 au in the *Voyager 1* direction. This is interpreted as the entering locations for real galactic protons in order to reach the hypothetical *Voyager 1* position at 145 au. Right plots show the results as $\kappa_{\parallel}/\kappa_{\perp}$ is increased by 10^{10} in the LISM. For comparison, the left plots show the results when no modification is made to this ratio. And the simulation outer boundary is set at 300 (1000) au for the two upper (lower) plots.

In the two lower plots of Figure 7, the simulation outer boundary is expanded to 1000 au. As shown in the lower left plot, if $\kappa_{\parallel}/\kappa_{\perp}$ is not increased, the probability for pseudo-particles exiting from the nose region is roughly the same as that of the tail region (different from the upper left plot). This is probably because the HMF spiral lines cannot extend fully from the nose region to the tail region at 1000 au. Only after this ratio is increased by 10^{10} and $\kappa_{\parallel}$ reaches 10^{27} cm^2 s^{-1} in the outer heliosheath is the tail region more occupied by the exiting pseudo-particles (the lower right plot).

Besides the spatial location, we also analyzed the exit momentum of these pseudo-particles. Figure 9 shows the normalized distribution of the exit momentum of pseudo-particles that started at a "145 au location" with a momentum of 0.644 GeV/c (200 MeV). Two different cases are illustrated here: (1) increasing the ratio $\kappa_{\parallel}/\kappa_{\perp}$ in the outer heliosheath (black solid line), and (2) without any modification to this ratio (red dashed line). The figure demonstrates that as this ratio is increased in the outer heliosheath (case 1), nearly all pseudo-particles experience no momentum change. From a modulation point of view, this is interpreted as galactic protons that entered the heliosphere with the same momentum as that observed, being unmodulated. These simulation results support the following scenario: after choosing a realistic parameter setup in the outer heliosheath, more CR protons diffuse along the magnetic field spiral lines from the tail region to the nose region, and the plasma environment encountered causes no momentum change. This is due to the fact that particles do not get inside the supersonic solar wind region, where adiabatic cooling happens. The details, for example, of what specific magnetic field structure supports this kind of transport process and if there is any particular requirement for the diffusion coefficient, will be explored further in a future study.

Figure 10 illustrates the exit locations of pseudo-particles that started from the LISM; for the two upper panels the starting point is 155 au; for the two lower panels it is 160 au in the *Voyager 1* direction. The plots on the left side show the results with no modification for $\kappa_{\parallel}/\kappa_{\perp}$, whereas the plots on the right side show the results when we increase this ratio by 10^{10} in the outer heliosheath. The plots on the right side illustrate that after $\kappa_{\parallel}/\kappa_{\perp}$ is magnified, nearly all the pseudo-particles exit at just two points on the simulation boundary. In this context, it is noted that in our MHD model, the IMF is set to be

$$\boldsymbol{B}_{\rm ISM} = -2.47\hat{i} + 0.803\hat{j} - 1.5\hat{k}\ \mu G; \qquad (10)$$

which is pointing to the negative X and Z axes. In Figure 8, the plot on the right side demonstrates how this IMF is oriented

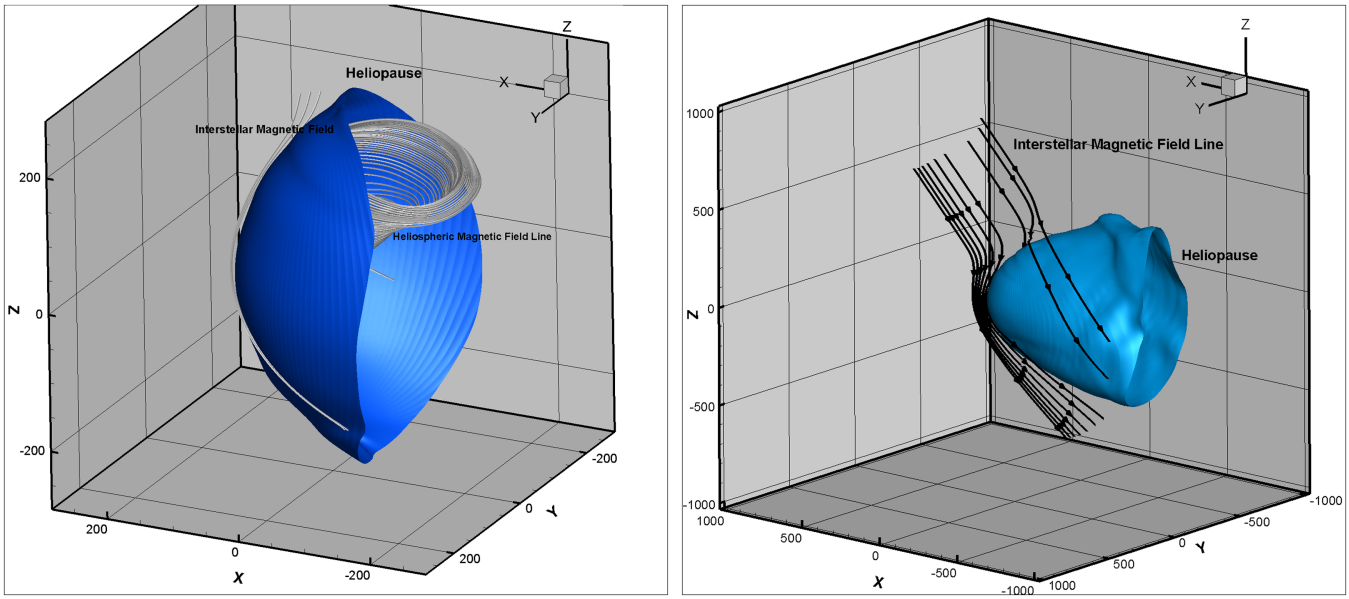


Figure 8. HMF and IMF line topologies near the HP in the MHD model. The unit for distance is au. The HP is resolved in different scales. The left panel demonstrates the case when the simulation outer boundary is set at 300 au. The HP is partially included in the left panel, since some tail region of the heliospheric is cut through by the simulation outer boundary. The simulation outer boundary of the right panel is set at 1000 au, most part of the helioshere is included in the simulation domain and the global heliospheric structure is more clearly demonstrated.

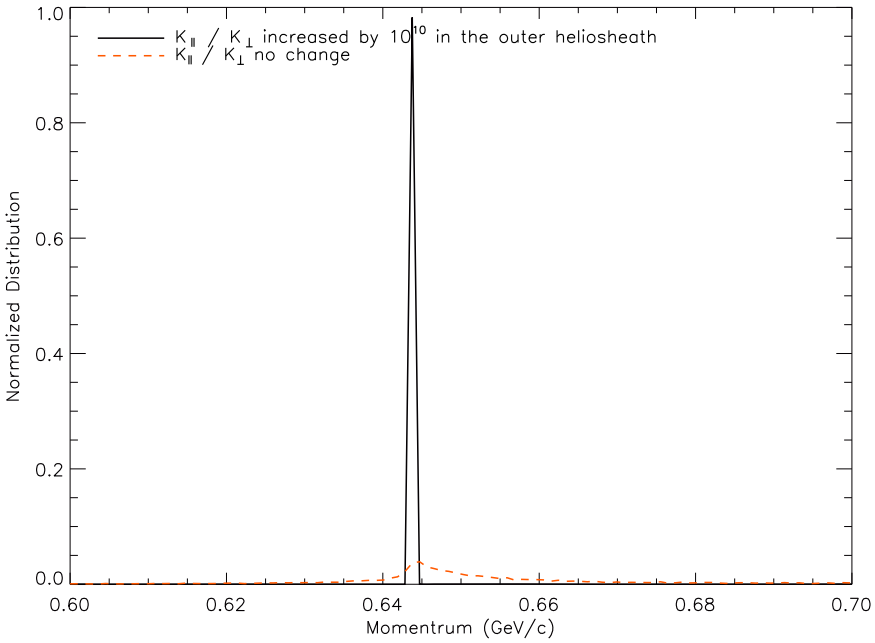


Figure 9. Normalized distribution of the exit momentum for 200 MeV (0.644 GeV/c) pseudo-particles that started at a radial distance of 145 au in the *Voyager 1* direction. The black solid line is for the case with $\kappa_{\parallel}/\kappa_{\perp}$ increased by 10^{10} in the outer heliosheath; the red dashed line shows the case with no modification of this ratio.

and draped around the HP. The two exit locations mentioned are roughly along the same direction as this IMF. In other words, by increasing the ratio of the diffusion coefficients, parallel diffusion dominates the transport and pseudo-particles mostly follow the magnetic field line. The Larmor radius R_L for 200 MeV proton in the IMF with a magnitude of 3 μG is about 0.04 au. With the increased ratio of $\kappa_{\parallel}/\kappa_{\perp}$, the diffusion coefficient beyond the HP is on the order of $\kappa_{\parallel} \simeq 10^{27}\,\mathrm{cm^2 s^{-1}}$, which gives a mean-free path of 10^4 au (10^5 times larger than the Larmor radius). If these pseudo-particles are considered to be CR particles, they simply keep gyrating along the magnetic field lines. And CR particles with small pitch angles to the magnetic field tend to travel more easily to the observer. This gives some hint as to why the observed CR anisotropy by *Voyager 1* is bidirectional (Krimigis et al. 2013; Strauss & Fichtner 2014; Strauss et al. 2015).

Based on the above results and argument, we come to a simple picture for how galactic CRs may propagate to

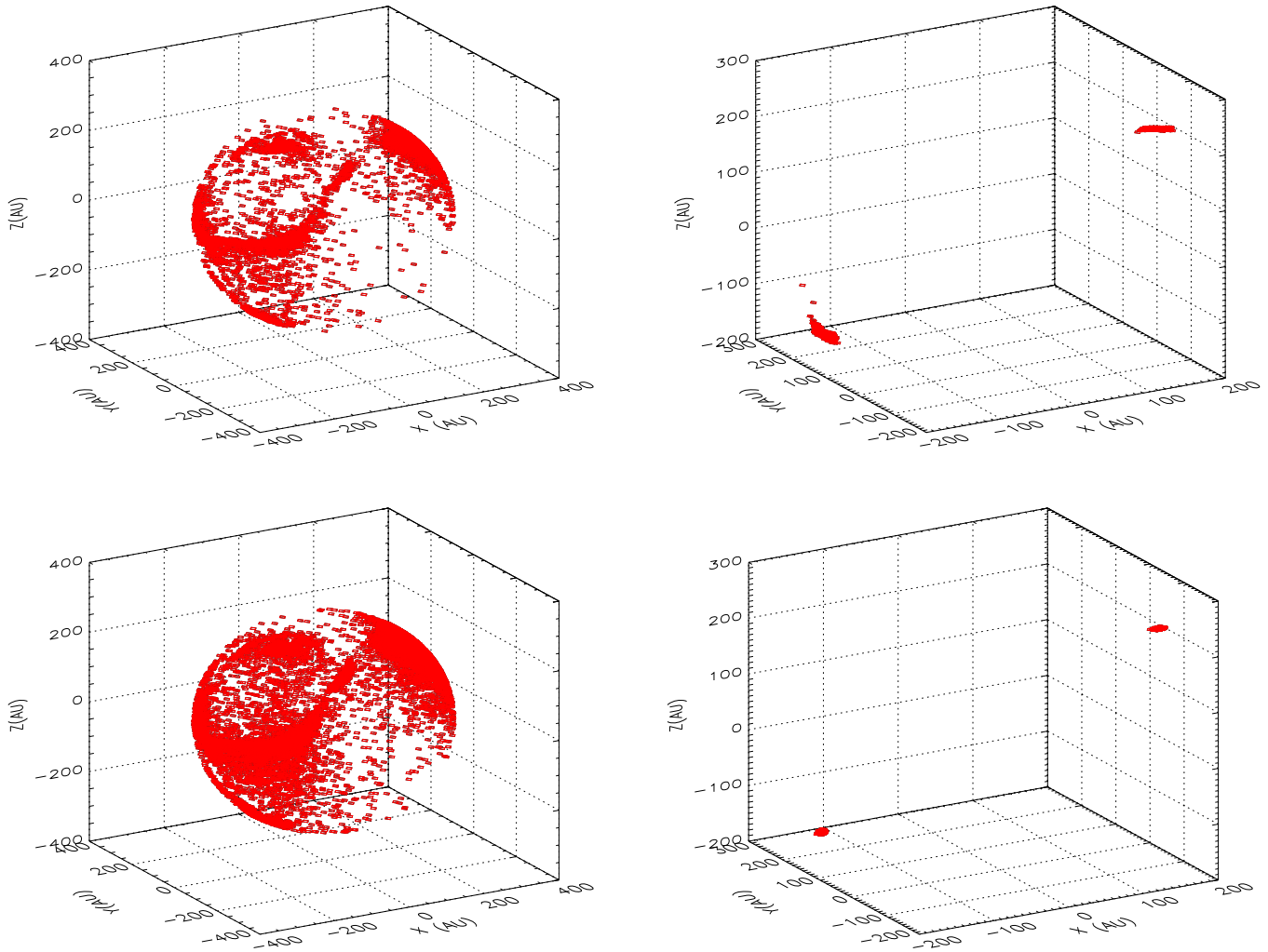


Figure 10. Similar to Figure 7 where the red points depict the exit locations of 200 MeV pseudo-particles, for the two upper (lower) plots with a starting point at 155 (160) au. Left plots show the results with no modification for $\kappa_{\parallel}/\kappa_{\perp}$, whereas the right plots show the results when $\kappa_{\parallel}/\kappa_{\perp}$ ratio is increased by 10^{10} in the outer heliosheath.

Voyager 1 near the HP; they arrive at the HP through propagation along the galactic magnetic field lines and reach the spacecraft either from the heliospheric nose region or from the tail region by parallel diffusion.

4. SUMMARY

In this paper, using a hybrid CR transport model and a parameter setup tuned to reproduce the *Voyager 1* galactic CR observations near the HP, we simulate the radial flux along different heliospheric directions. It was found that the flux variation along the *Voyager 2* direction exhibits a clear flux jump near the HP, which could be used as a signature of the spacecraft crossing the HP. These intensity jumps cannot be reproduced by simple modulation models that prescribe the LIS at the HP and assume it to be the modulation boundary. Therefore, although modulation beyond the HP may be judged to be almost negligible, the outer heliosheath must be included in the modulation model to accurately describe CR transport near and across the HP. Such large flux jumps to reach the interstellar values are not found in the polar and downwind directions. Our simulations also indicate that in the polar regions and particularly in the tail region, a well-defined thin HP layer, between the solar wind and the LISM, is less likely than in the nose direction. The CR flux is influenced by flows from both LISM and heliospheric sides over tens of au in this region.

Assuming a constant speed for *Voyager 2*, scaling the MHD location of the HP and TS to *Voyager 1* and *2* observations, we predict that the HP should be around 115 au along the *Voyager 2* direction. This corresponds to a crossing of the HP by *Voyager 2* in 2017 February.

We also investigated whether the HP can be considered the true modulation boundary, performing simulations for 200, 50, 10, and 5 MeV galactic protons in the *Voyager 1* direction. When using $K_{\parallel} \simeq 10^{27}\,\mathrm{cm^2\,s^{-1}}$, $K_{\perp} \simeq 10^{17}\,\mathrm{cm^2\,s^{-1}}$, $K_{rr} \simeq 10^{26}\,\mathrm{cm^2\,s^{-1}}$, we found that there is a modest modulation beyond the HP, seemingly only over the first 10 au beyond the HP, contributing less than 1% to the total modulation. The *Voyager 1* CR observations beyond the HP thus enable us to obtain the LIS. Together with the higher energy end of the CR spectrum as constrained by the PAMELA experiment (Potgieter et al. 2014, 2015), the very local interstellar spectrum for protons from 1 MeV to 100 GeV is known (Potgieter 2014; Bisschoff & Potgieter 2015; Vos & Potgieter 2015).

We analyzed the exit spatial positions (momentum) of pseudo-particles, interpreted as the heliospheric entering positions (momentum) for CR particles. We find that many

particles arriving at the heliospheric nose region come from the tail region. We proposed that the HMF line topology and configuration may play an important role in setting up such an effect. The HMF lines, which intersect the simulation outer boundary in the tail region, connect to the nose region. Thus, in our simulation, it is found that many pesudo-particles observed in the nose region will follow these HMF spiral lines and exit from the tail region.

Finally, our simulations demonstrate an anisotropic characteristic in the CR flux beyond the HP. After increasing the ratio $\kappa_{\parallel}/\kappa_{\perp}$ by 10^{10}, the exit locations of pseudo-particles, which started from the LISM (at 155 or 160 au), are along the prescribed IMF direction as in the MHD model. With a very large parallel mean free path, the CR particles simply follow the magnetic field lines to propagate in the LISM.

The work is jointly supported by the National Basic Research Program (973 program) under grant 2012CB825601, the Knowledge Innovation Program of the Chinese Academy of Sciences (KZZD-EW-01-4), the National Natural Science Foundation of China (41231068, 41304137, 41274192, 41374188, 41531073, and 41504132), and the Specialized Research Fund for State Key Laboratories. X.L. acknowledges the support of the post-doctoral programme of the North-West University in South Africa. M.P. acknowledges the financial support of the South African National Research Foundation (NRF) under the Incentive and Competitive Funding for Rated Researchers, grants 87820 and 68198. M.Z. and N.P. were supported, in part, by NASA grants NNX12AB30G, NNX14AJ53G, NNX15AN72G, and NNX14AF41G. MHD simulations were supported through NSF PRAC award OCI-1144120 and related computer resources from the Blue Waters sustained petascale computing project. N.P. also acknowledges supercomputer time allocations provided on SGI Pleiades by NASA High-End Computing Program award SMD-11-2195 and Cray XT5 Kraken by the NSF XSEDE project MCA07S033. M.Z., M.P., R.D.S., and N.P. appreciate discussions at the team meeting Heliosheath Processes and Structure of the Heliopause: Modeling of Energetic Particles, Cosmic Rays, and Magnetic Fields supported by the International Space Science Institute in Bern, Switzerland.

REFERENCES

Bisschoff, D., & Potgieter, M. S. 2015, Ap&SS, 361, 48
Burlaga, L. F., Ness, N. F., Florinski, V., & Heerikhuisen, J. 2014, ApJ, 792, 134
Burlaga, L. F., Ness, N. F., Gurnett, D. A., & Kurth, W. S. 2013, ApJL, 778, L3
Florinski, V., Jokipii, J. R., Alouani-bibi, F., & Le Roux, J. A. 2013, ApJL, 776, L37
Florinski, V., Stone, E. C., Cummings, A. C., & Le Roux, J. A. 2015, ApJ, 803, 47
Gamayunov, K., Zhang, M., & Rassoul, H. 2010, ApJ, 725, 2251
Gurnett, D. A., Kurth, W. S., Stone, E. C., et al. 2015, ApJ, 809, 121
Gurnett, D. A., Kurth, W. S., Burlaga, L. F., & Ness, N. F. 2013, Sci, 341, 1489
Intriligator, D. S., Sun, W., Dryer, M., et al. 2015, JGR, 120, 8267
Jokipii, J. R., & Kóta, J. 2014, ApJL, 794, L4
Kopp, A., Büsching, I., Strauss, R. D., & Potgieter, M. S. 2012, CoPhC, 183, 530
Kóta, J., & Jokipii, J. R. 2014, ApJ, 782, 24
Krimigis, S. M., Decker, R. B., Roelof, E. C., et al. 2013, Sci, 341, 144
Luo, X., Zhang, M., Potgieter, M. S., Feng, X., & Pogorelov, N. V. 2015, ApJ, 808, 82
Luo, X., Zhang, M., Rassoul, K. H., Pogorelov, N. V., & Heerikhuisen, J. 2013, ApJ, 764, 85
McComas, D. J., & Schwadron, N. A. 2012, ApJ, 758, 19
Parker, E. N. 1965, P&SS, 13, 9
Pogorelov, N. V., Suess, S. T., Borovikov, S. N., et al. 2013, ApJ, 772, 2
Potgieter, M. S. 2014, BrJPh, 44, 581
Potgieter, M. S., Vos, E. E., Boezio, M., et al. 2014, SoPh, 289, 391
Potgieter, M. S., Vos, E. E., Munini, R., Boezio, M., & Di Felice, V. 2015, ApJ, 810, 2
Richardson, J. D., & Decker, R. B. 2014, ApJ, 792, 126
Scherer, K., Fichtner, H., Strauss, R. D., et al. 2011, ApJ, 735, 128
Stone, E. C., Cummings, A. C., McDonald, F. B., et al. 2008, Natur, 454, 71
Stone, E. C., Cummings, A. C., McDonald, F. B., et al. 2013, Sci, 341, 150
Strauss, R. D., & Fichtner, H. 2014, A&A, 572, L3
Strauss, R. D., & Potgieter, M. S. 2014, AdSpR, 53, 1015
Strauss, R. D., Fichtner, H., Potgieter, M. S., Le Roux, J. A., & Luo, X. 2015, JPhCS, 642, 012026
Strauss, R. D., Potgieter, M. S., Ferreira, S. E. S., Fichtner, H., & Scherer, K. 2013, ApJL, 765, L18
Strong, A. W., Moskalenko, I. V., & Ptuskin, V. S. 2007, ARNPS, 57, 285
Vos, E. E., & Potgieter, M. S. 2015, ApJ, 815, 119
Webber, W. R., & Intriligator, D. S. 2015, arXiv:1502.01307
Webber, W. R., & McDonald, F. B. 2013, GeoRL, 40, 1665
Webber, W. R., & Quenby, J. J. 2015, ApJ, 806, 138
Zhang, M. 1999, ApJ, 513, 409
Zhang, M., Luo, X., & Pogorelov, N. V. 2015, PhPl, 22, 091501